Žibert T, Likozar B, Huš M. Pristine and ruthenium-doped TiO [sub] 2 nanoclusters for nitrogen reduction reaction : Ab initio study of structure and adsorption. *Fuel*. 2023;(334):1-11. doi:10.1016/j.fuel.2022.126451

Pristine and ruthenium-doped TiO_2 nanoclusters for nitrogen fixation: First-principles modeling of structure and adsorption

Taja Žibert[a,b], Blaž Likozar[a,*], Matej Huš[a,b,c,**]

[a]*National Institute of Chemistry, Department of Catalysis and Chemical Reaction Engineering, Hajdrihova 19, SI-1001 Ljubljana, Slovenia*
[b]*University of Nova Gorica, Vipavska 13, SI-5000 Nova Gorica, Slovenia*
[c]*Association for Technical Culture (ZOTKS), Zalos̆ka 65, SI-1001 Ljubljana, Slovenia*

Abstract

The Haber-Bosch process has been the workhorse of ammonia synthesis for more than a century, but its environmental cost has instigated the search for greener methods of nitrogen activation. Photocatalysis using doped titanium dioxide (TiO_2) stands out as a promising method. In this work, we explore the electronic properties of pristine and Ru-loaded TiO_2 clusters and the activation of nitrogen, hydrogen and ammonia on these clusters. We study the effect of the cluster size and the role of Ru on the electronic properties of the clusters and their activation capabilities. We show that loading with Ru enhanced the nitrogen fixation ability, yet it does not influence the adsorption of hydrogen and ammonia, avoiding catalyst poisoning.

Keywords: nitrogen fixation, titanium dioxide, ruthenium, surface adsorption characteristics, density functional theory

1. Introduction

Ammonia synthesis has attracted considerable attention ever since the Haber-Bosch (HB) process was invented more than a century ago. Ammonia is used extensively in the production of fertilizers, as a precursor in the chemical industry, for explosives and as a chemical energy storage [1–3]. Ammonia synthesis with the conventional Haber-Bosch process requires hydrogen as one of

*Corresponding author
**Corresponding author
Email addresses: blaz.likozar@ki.si (Blaž Likozar), matej.hus@ki.si (Matej Huš)

the reactants, which is usually obtained from natural gas by steam reforming [4, 5]. This results in significant carbon dioxide emissions. Combined with high required temperature and pressure for nitrogen activation, makes the HB process environmentally unfriendly. Hence, alternative ways of activating nitrogen by using (solar) light as the driving force for nitrogen reduction reaction (NRR) are sought for [6, 7].

TiO_2 is a transition metal oxide used in a variety of applications, including cosmetics, the food industry, solar cells, catalysts, etc. [8]. In nature, it occurs in three crystalline phases, namely as rutile, anatase and brookite. Among them, anatase exhibits the best (photo)catalytic activity, while rutile is thermodynamically the most stable [8–10]. It is the archetypal photocatalyst because of its ubiquitousness. It has been used for water splitting [11, 12], CO_2 reduction [9] and N_2 fixation [13]. While TiO_2 is popular due to its high chemical stability, high surface area, photocatalytic activity, non-toxicity, and low cost, making it a benchmark catalyst [8, 9], it has a band gap that is too large to efficiently utilize the visible light. The band gap of $\sim$ 3 eV (3.03 eV for bulk rutile and 3.20 eV for anatase) [14] is suitable to utilize ultraviolet light (UV). It can be reduced, improving the photocatalytic properties, by introducing defects (such as oxygen vacancies) and/or dopant atoms or creating heterostructures (combined catalysts) [6].

Nitrogen fixation under photocatalytic conditions was first reported by Schrauzer and Guth in their seminal paper in 1977, using titanium dioxide (TiO_2) as a photocatalyst [15]. Since then, a diverse range of photocatalysts have been tested for ammonia synthesis, including metal oxides (TiO_2), g-C_3N_4, bismuth oxyhalides, sulfides etc.[16]. Titanium dioxide is still widely used for photocatalytic nitrogen fixation. Many theoretical calculations have been performed to investigate the NRR over TiO_2-based photocatalysts. Several experimental-theoretical [17–35] or theoretical studies [36] have reported optical and electronic properties and studied the reaction mechanism over pristine and doped TiO_2 photocatalysts. For instance, Ghoshal et al.[37] studied nitrogen fixation with H_2O over TiO_2-doped Ru_n (n = 5 and 6) clusters and calculated the energetics and kinetics of the mechanisms of NRR: distal, alternating, and enzymatic.

In this paper we systematically study nitrogen fixation over differently sized $(TiO_2)_n$ and Ru-$(TiO_2)_n$ clusters ($n = 1 - 12$) using density functional theory (DFT). The most energetically favor-

able TiO_2 clusters were geometrically optimized and their thermodynamic stability was confirmed by *ab initio* molecular dynamics simulations (AIMD). The Ru atom was loaded on TiO_2 clusters in the global minima, as confirmed by testing different possibilities and performing AIMD. Studying the adsorption modes of the nitrogen molecule (N_2), hydrogen atom (H), and ammonia molecule (NH_3) showed a clear size effect. We show that loading with Ru enhanced the nitrogen fixation ability, yet it does not influence the adsorption of hydrogen and ammonia, avoiding catalyst poisoning.

2. Methods

Density functional theory (DFT) calculations were performed in the GPAW [38, 39] environment. Using the plane-wave formalism with periodic boundary conditions, electron-core interactions were described with projector augemented wave method (PAW) pseudopotentials. The PBE [40] functional within the generalized gradient approximation (GGA) was used for geometry optimization and to study the adsorption of hydrogen, nitrogen, and ammonia. The hybrid HSE06 functional [41] was used to calculate the electronic properties in single-point passes because of its superiority towards GGA[42, 43]. The plane wave basis set with a cut-off energy of 500 eV was used. The converge convergence criteria for the energy and forces on all individual atoms (fmax) were set to 0.0005 eV/electron and 0.01 eV/Å, respectively. TiO_2 and Ru-TiO_2 clusters were enclosed in simulation cells of varying sizes with at least of 10 Å vacuum in each direction. Only one K point was sampled (Γ). Fermi-Dirac smearing of 0.001 eV was used for all calculations.

2.1. Geometry optimization of clusters

2.1.1. $(TiO_2)_n$ clusters

The initial configurations of $(TiO_2)_n$ clusters ($n = 1 - 12$) were adopted from Berardo et al. [44] and Çakir et al. [10], and re-optimized for consistency. For larger clusters, additional configurations were discovered by the ABCcluster software [45–47], which was used to ensure that all possible structures were considered. We list them in the SI.

The formation energies of TiO_2 clusters ($E\,(TiO_2)_{form}$) per a TiO_2 unit relative to the optimized TiO_2 monomer ($n = 1$) were calculated, as follows:

$$E\,(TiO_2)_{form} = E_n/n - E_1 \tag{1}$$

where E_n denotes the total energy of the $(TiO_2)_n$ cluster, n is the cluster size and E_1 total energy of the monomer [10]. The formation energies of TiO_2 clusters relative to bulk rutile or anatase were calculated as

$$E\,(TiO_2)_{cluster} = E_n/n - E_{bulk}/m \tag{2}$$

where E_{bulk} stands for the energy of optimized geometry of bulk rutile or anatase with m TiO_2 in the unit cell.

2.1.2. Ru-$(TiO_2)_n$ clusters

Ru-TiO_2 clusters were generated by adding a single Ru atom to the most stable of each $(TiO_2)_n$ clusters. For larger clusters, several positions were tested to find the true global minimum. Their formation energies $E\,(Ru(TiO_2)_n)_{form}$ were calculated as

$$E\,(Ru(TiO_2)_n)_{form} = E_{Ru(TiO_2)_n} - E_{(TiO_2)_n} - E_{Ru} \tag{3}$$

where $E_{Ru(TiO_2)_n}$ denotes the total energy of the Ru-$(TiO_2)_n$ cluster, $E_{(TiO_2)_n}$ the total energy of a $(TiO_2)_n$ cluster and E_{Ru} the total energy of a single Ru atom. The formation energies of $Ru(TiO_2)_n$clusters relative to bulk ruthenium were calculated as

$$E\,(Ru(TiO_2)_n)_{cluster} = E_{Ru(TiO_2)_n}/n - E_{TiO_2} - E_{Ru,bulk}/m \tag{4}$$

where $E_{Ru,bulk}$ stands for the energy of bulk ruthenium and m the number of ruthenium atoms in the unit cell.

Table 1 shows the number of valence electrons for each TiO_2 and Ru-TiO_2 cluster.

Table 1: Number of valence electrons of TiO_2 and Ru-(TiO_2) clusters

$(TiO_2)_n$ clusters, n	$n_{valence\ electrons}$	Ru-$(TiO_2)_n$ clusters, n	$n_{valence\ electrons}$
1	24	1	40
2	48	2	64
3	72	3	88
4	96	4	112
5	120	5	136
6	144	6	160
7	168	7	184
8	192	8	208
9	216	9	232
10	240	10	256
11	264	11	280
12	288	12	304

2.1.3. Ab initio Molecular Dynamics Simulations

Thermodynamic stability of TiO_2 and Ru-TiO_2 clusters was confirmed by *Ab Initio* Molecular Dynamics (AIMD). The AIMD calculations were performed in plane-wave mode with an energy cutoff of 500 eV, PBE functional, at the gamma point and with a Fermi-Dirac smearing of 0.001 eV. Simulations were carried out at a temperature of 1500 K for 0.2 ps and a time step of 0.1 fs. The energy convergence was set to 0.0005 eV/electron and the force convergence to 0.01 eV/Å. The Berendsen thermostat was used to ensure a constant temperature during the simulations. Clusters that remained stable during the AIMD were retained for further investigation.

2.2. Adsorption

The adsorption modes of H, N_2 and NH_3 were calculated on the preoptimized structures of $(TiO_2)_n$ and Ru-$(TiO_2)_n$ ($n = 3, 6, 12$) clusters. For isolated adsorbates, their structures were optimized in a box with at least of 10 Å vacuum in each dimension. The adsorption energies (E_{ads}) were calculated as

$$E_{ads} = E_{cluster+adsorbed\ species} - (E_{cluster} + E_{isolated\ species}) \quad (5)$$

where $E_{cluster+adsorbed\ species}$ denotes the total energy of H, N_2 or NH_3 adsorbed on the TiO_2 or Ru-TiO_2 clusters, respectively, $E_{cluster}$ the total energy of the isolated cluster and $E_{isolated\ species}$ the total

energy of isolated N_2 or NH_3. For H adsorption, we report the results relative to $\frac{1}{2}H_2$. To check for pairing effects, adsorption of 2 H over TiO_2 and Ru-TiO_2 clusters was also studied.

3. Results and discussion

3.1. Optimized structures

3.1.1. $(TiO_2)_n$ clusters

While TiO_2 crystallizes in several polymorphs (rutile, anatase, brookite) [8], smaller clusters can exhibit better catalytic properties. It has been shown many times that nanoparticles are more active than extended surfaces because their atoms are under-coordinated [48, 49]. Hence, we study different TiO_2 nanoparticles to obtain better insight into structure-property relations and to determine the active sites, which could participate in the NRR mechanism [10, 37]. The determined putative global-minima structures of $(TiO_2)_n$ $n = 3, 6, 12$ are shown in Figure 1 and in the SI for the other sizes ($n < 12$).

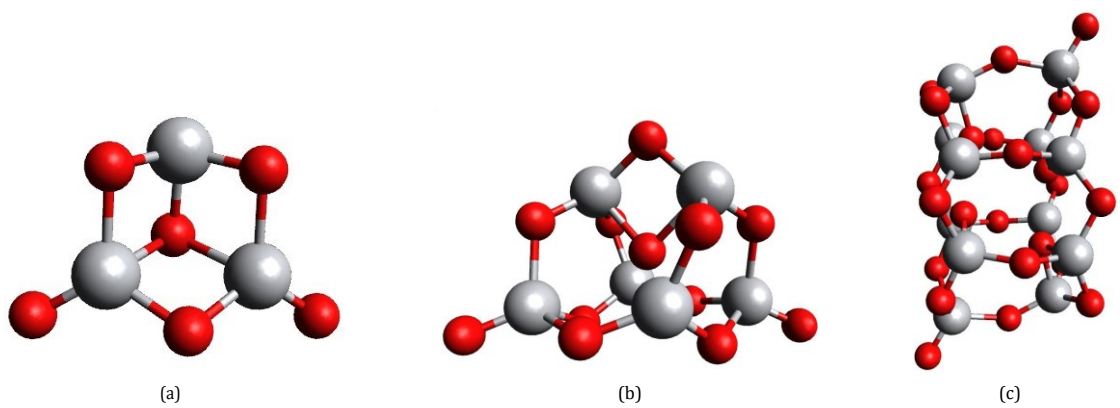

Figure 1: Optimized putative global-minima structures of a) $(TiO_2)_3$, b) $(TiO_2)_6$ and c) $(TiO_2)_{12}$ clusters.

In small clusters, the atoms are undercoordinated and therefore more reactive towards adsorbates and each other. While a typical shortest Ti-O distance in rutile and anatase is 1.69 and 1.97 Å, respectively, it is reduced in nanoparticles. For the smallest studied clusters, these values range from 1.65, 1.64–1.86 and 1.64–2.09 Å for $n = 1, 2, 3$, respectively. The atoms in clusters are not equivalent as opposed to bulk rutile and anatase.

Small TiO_2 clusters have considerably larger energy (per atom) than bulk TiO_2, meaning that they are more reactive. We studied the size dependence of TiO_2 clusters energy to ascertain their relative stability. In Figure 2, we list the formation energies of $(TiO_2)_n$, $n = 1 - 12$, clusters relative to a TiO_2 monomer, rutile and anatase. As expected, larger clusters are progressively more stable and lower-lying in energy. For larger clusters ($n > 10$), stabilization increment per $(TiO_2)_1$ added is 4.73 eV. The results agree well with the results reported by Çakir et al. [10]. Furthemore, we show the highest occupied molecular orbital (HOMO) and the lowest unoccupied molecular orbital (LUMO) of $(TiO_2)_6$ cluster (Figure 3). HOMO and LUMO molecular orbitals can be used to predict which part of the cluster acts as a nucleophile and which as an electrophile. HOMO is the fully occupied orbital and can be considered as a nucleophile that can be attracted to the electrophile and vice versa for the LUMO orbital.

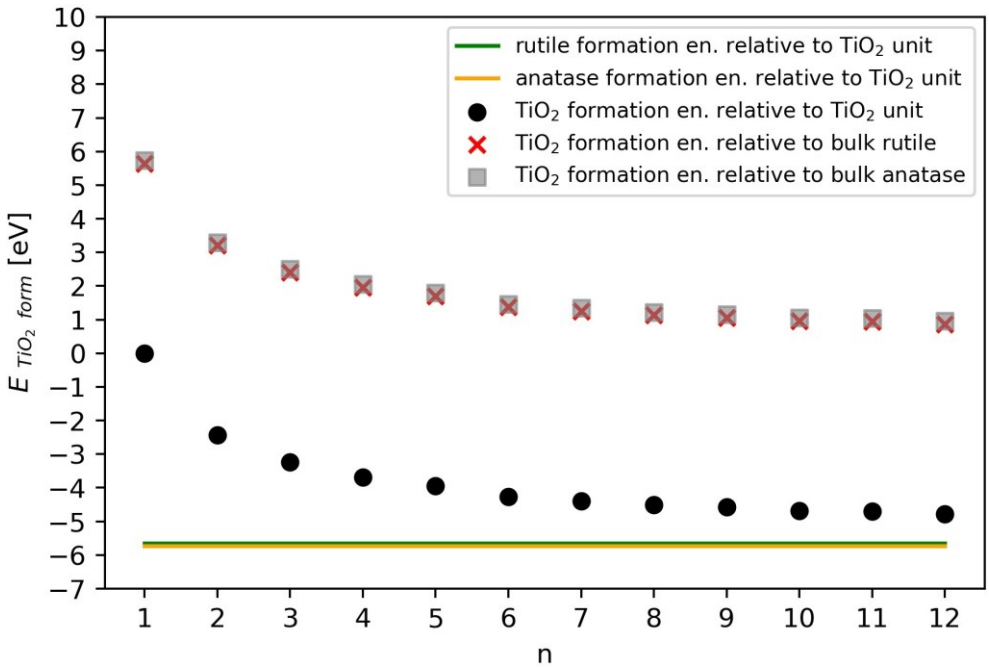

Figure 2: Formation energies of TiO_2 clusters relative to a TiO_2 monomer, and bulk anatase and rutile calculated with the PBE functional.

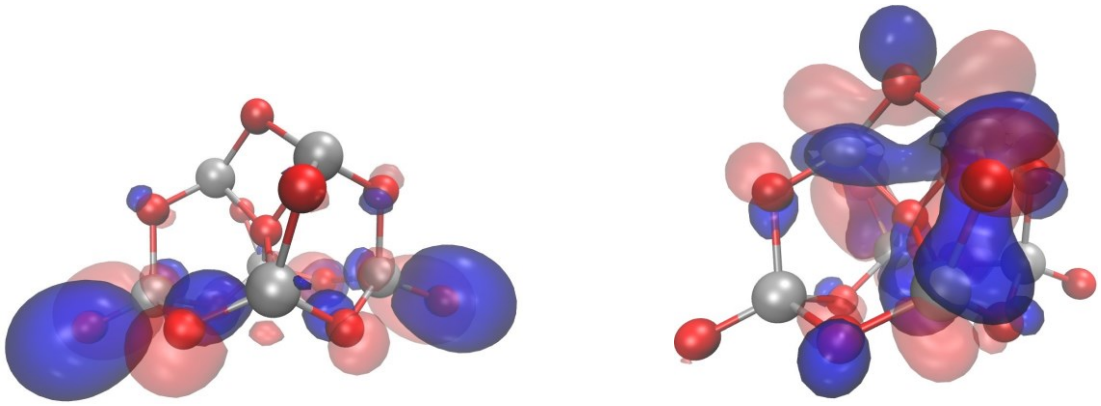

(a) (b)

Figure 3: a) HOMO and b) LUMO orbitals of the $(TiO_2)_6$ cluster at an isovalue of $\pm$ 0.02 $e_0/Å^3$.

3.1.2. Ru-$(TiO_2)_n$ clusters

Transition metals are commonly used in photocatalysis to improve the structural, electronic, and/or photocatalytic properties of the desired catalyst. Heteroatoms can be doped into the bulk structure or loaded onto the surface of the catalyst. Furthermore, heterojunctions, *i.e.*, the combination of two different semiconductors, can be formed [16]. Herein, we loaded a single Ru atom on the surface of the studied TiO_2 clusters. For nanoclusters, the difference between surface loading and bulk doping becomes elusive. As we show later on, the configuration of a single Ru atom and a nanocluster is energetically favourable and such structures are stable.

The most stable structures of Ru-$(TiO_2)_n$ clusters were determined for $n = 1 - 12$. In Figure 4, we depict these for $n = 3, 6, 12$, while the remaining structures can be found in the Supplementary Information (Figure S3). We see that loading Ru does not noticeably perturb the structure of TiO_2 clusters. In smaller clusters Ru binds to oxygen and titanium atoms, while in larger clusters it binds preferentially to titanium atoms. To determine the relative stability of the Ru-TiO_2 clusters, their formation energies relative to a single Ru or to bulk ruthenium and barren $(TiO_2)_n$ clusters were calculated (Figure 5). In general, the Ru atoms are more stabilized on larger clusters but there are outliers. While the formation energy of the $(TiO_2)_n$ clusters monotonically decreases (per formula unit), the situation is more complex for Ru-$(TiO_2)_n$. The formation energy is also

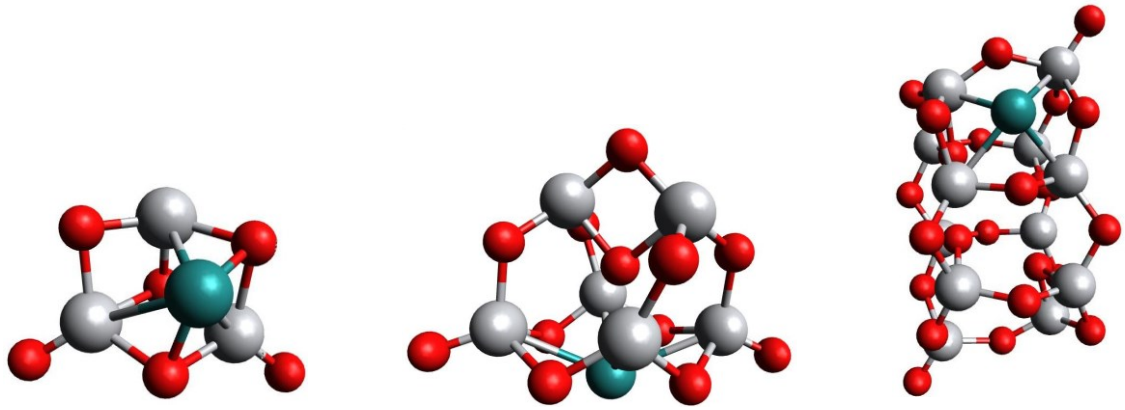

(a) (b) (c)

Figure 4: Optimized structures of the a) Ru-$(TiO_2)_3$, b) Ru-$(TiO_2)_6$ and c) Ru-$(TiO_2)_{12}$ clusters.

influenced by geometric effects, in particular the number of Ru-O and Ru-Ti bonds. Ru-$(TiO_2)_5$ is thus a notable outlier with a very favourable formation energy because it forms three strong Ru-O bonds with terminal oxygen atoms (see SI).

In addition to the most stable loadings of Ru, some other tested configurations are also shown. Among the tested nanoparticles, $(TiO_2)_5$ is thermodynamically most stable with a Ru atom. Since the degree of hydroxylation of the cluster and the role of oxygen vacancies is herein not explored, the most stable TiO_2 and Ru-TiO_2 clusters under relevant thermodynamic conditions under which ammonia synthesis is performed might differ. For the Ru-$(TiO_2)_6$ cluster, the HOMO and LUMO are shown in Figure 6.

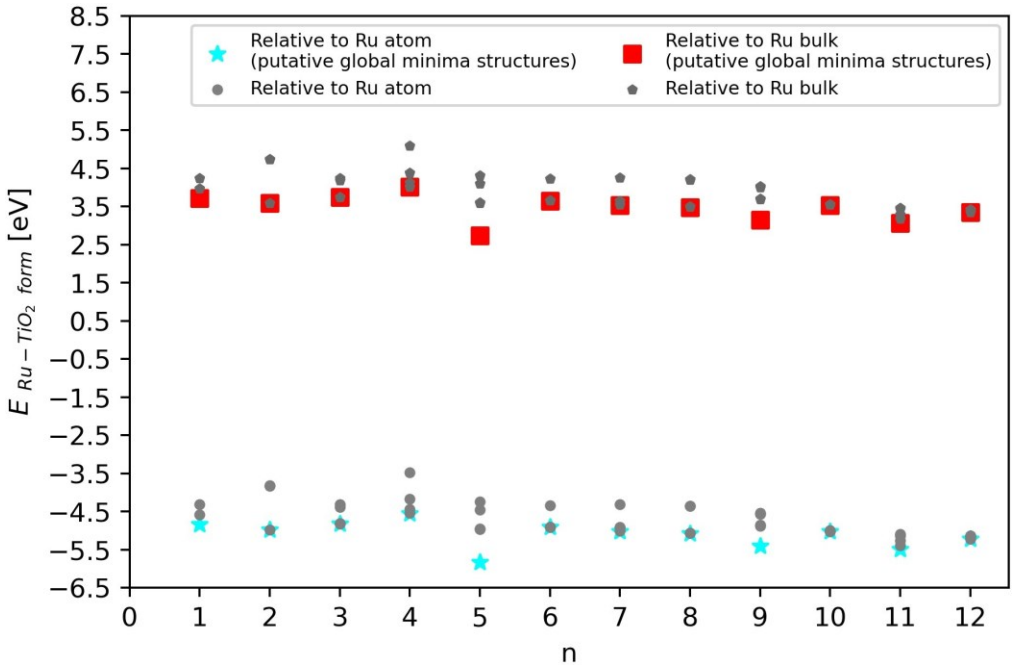

Figure 5: Energies of Ru loading for Ru-TiO_2 clusters relative to a single Ru atom and bulk ruthenium (and the correspond- ing $(TiO_2)_n$ cluster) calculated with the PBE functional. For each cluster size (n) energies of the clusters with different Ru positions are shown.

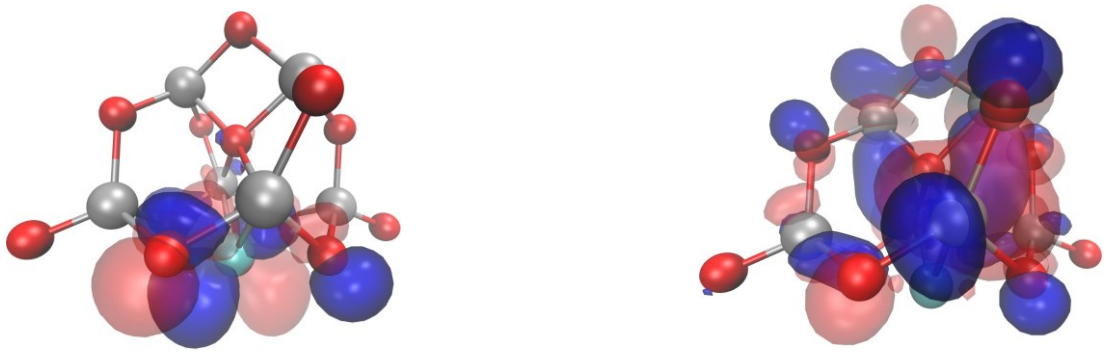

(a) (b)

Figure 6: (a) HOMO and (b) LUMO orbitals of the Ru-$(TiO_2)_6$ cluster at an isovalue of $\pm$ 0.02 $e_0/\text{Å}^3$.

3.2. *Electronic properties*

The performance of materials for photocatalysis are in large part determined by their electronic properties. To evaluate the suitability of different Ru-$(TiO_2)_n$ nanoclusters, we first calculated their HOMO-LUMO gap, their Fermi level, (projected) density of states (PDOS) and, later on, adsorption energies. Since GGA functionals are known to describe semiconductors poorly, a hybrid functional (HSE06) was used for single-point calculations of electronic properties. We also plot the GGA results to show the discrepancies.

3.2.1. *$(TiO_2)_n$ clusters*

In small isolated systems (such as nanoclusters or molecules), the difference between HOMO and LUMO energy levels (the HOMO-LUMO gap) is analogous to the band gap crystalline semiconductors. The HOMO functions as the valence band and the LUMO features as the conduction band [50]. For the calculation of the HOMO-LUMO gap, the choice of the functional used during DFT calculations is of great importance. It is known that the electronic properties calculated using GGA-based functionals (for instance, PBE) can be qualitatively wrong. While hybrid functionals are a common approach aimed at alleviating these problem, they can be prohibitively expensive. Then, the DFT+U approach is used to obtain the reliable results [42, 43]. Both approaches suffer from transferrability issues as they use system-dependent parameters (mixing parameter in hybrid

functionals and the Hubbard U value in DFT+U).

The band gap in bulk rutile and anatase is 3.03 and 3.20 eV, respectively [12]. While loading TiO_2 with metals is known to depress its band gap [51, 52], isolated clusters in general have *higher* HOMO-LUMO gaps. The relations, however, are not monotonous. In our study, the HOMO-LUMO gaps were calculated using the GGA-based PBE and the hybrid HSE06 functional.

We see in Figure 7 that the HOMO-LUMO gaps for TiO_2 clusters range from 3.3 eV to 5.2 eV without a clear trend. While the PBE functional systematically underestimates the band gap in bulk rutile and anatase for ~1.3 eV, the difference for nanoclusters increases to ~1.5 eV. The lowest gap belongs to the $(TiO_2)_3$ and $(TiO_2)_9$ clusters (3.33 (HSE06) and 3.55 eV (HSE06) , respectively), while the highest to $(TiO_2)_{10}$ cluster (5.21 eV (HSE06)), which is consistent with the gaps obtained by Çakir et al. [10]. Despite intensive efforts, the HOMO-LUMO gap for $(TiO_2)_{12}$ cluster could not be computed at the HSE06 level due to electronic convergence problems.

These results show that TiO_2 nanoclusters utilize the far UV spectrum, while bulk TiO_2 is most active in near UV. These makes the former ill-suited for harvesting solar energy on Earth because that part of the spectrum is filtered out by the atmosphere. However, as it will be shown later on, doping with Ru makes them much more active in the visible range.

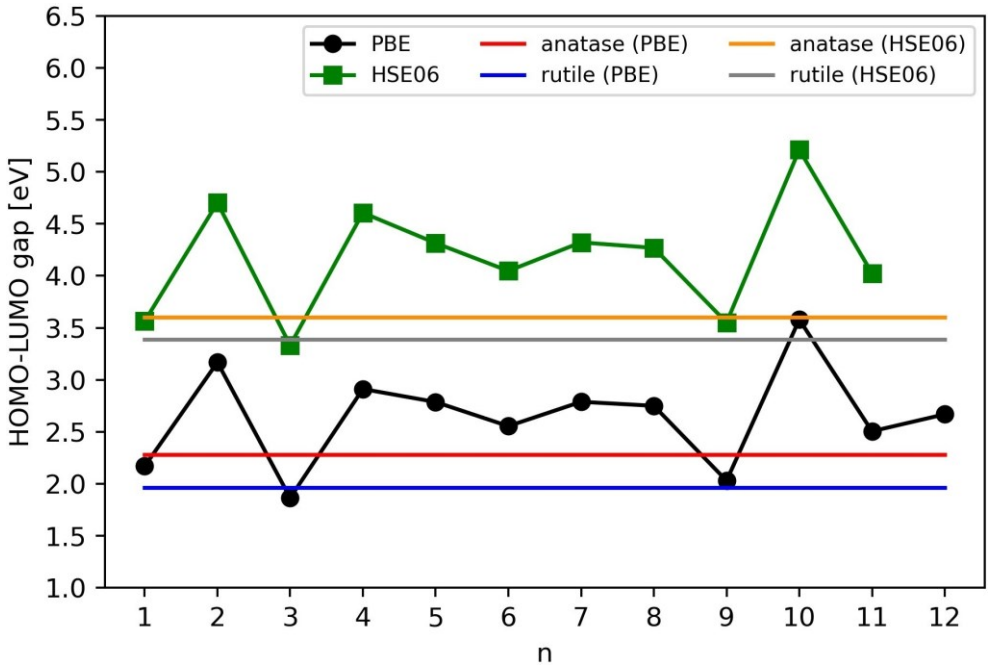

Figure 7: The HOMO-LUMO gap of $(TiO_2)_n$ clusters calculated with the PBE and HSE06 functionals. Band gap values for bulk rutile and anatase calculated with HSE06 functional are adopted from Landmann et al. [53].

For additional insight into the electronic structure of the TiO_2 clusters, we calculated the total density of states (DOS) and the projected density of states (PDOS) at the GGA and hybrid levels (Figure 8), all drawn relative to the Fermi level (0.0 eV). We show these properties for the $(TiO_2)_6$ cluster. PDOS provides detailed insight into the contribution of individual atoms and their distribution of their orbitals. We see that the states below the Fermi level (0.0 eV) are composed of oxygen p orbitals, while the states above the Fermi level consist mainly of Ti d orbitals, implying the relative composition of HOMO and LUMO. HOMO of $(TiO_2)_6$ is located at ~ -1.04 eV (PBE) or -1.7 eV (HSE06), while LUMO is found at ~ 1.5 eV (PBE) and 2.4 eV (HSE06). For the values of HOMO and LUMO for other clusters ($n = 1 - 12$) and the accompanying densities of states ($n = 3, 6, 12$), the reader is referred to the Supplementary Information.

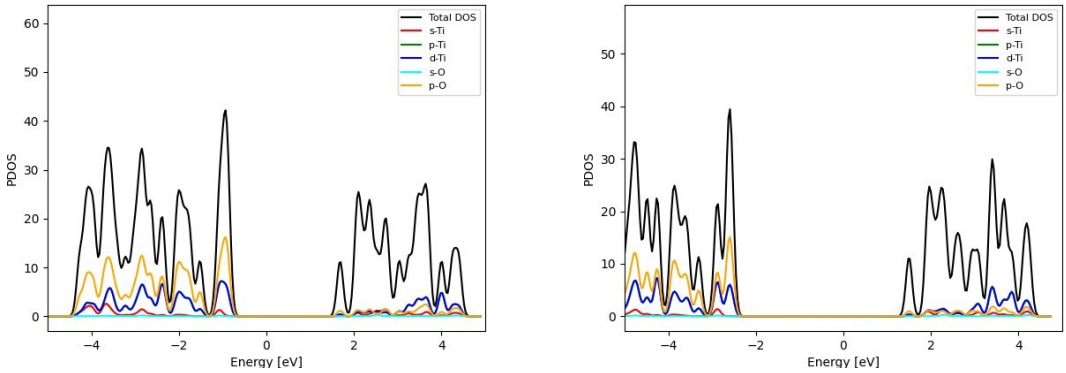

(a) PBE functional

(b) HSE functional

Figure 8: Total density of states and projected density of states of the $(TiO_2)_6$ cluster calculated with a) PBE and b) HSE06 functionals.

3.2.2. *Ru-$(TiO_2)_n$ clusters*

To be suitable for nitrogen fixation, TiO_2 nanoclusters can be doped with Ru. By doing so, we lower the HOMO-LUMO gap to utilize longer wavelengths (in the visible range of the spectrum) and tailor the catalytic properties. In Figure 9, we plot the HOMO-LUMO gaps of different Ru-$(TiO_2)_n$ ($n = 1 - 12$) clusters, calculated with the PBE and HSE06 functionals. As for pristine $(TiO_2)_n$ clusters, there is no simple relation between the cluster size and the band gap. We observe that the gap is smallest for $(TiO_2)_4$ and largest for $(TiO_2)_{11}$ (calculated with the PBE functional). This is not related to pristine (non-doped) clusters. The discrepancy between the PBE and HSE06 values is on average $\sim$ 1.5 eV, which is comparable to the difference calculated for the TiO_2 clusters. As a general observation, the HOMO-LUMO gap for Ru-doped clusters is on average 1.6 eV lower than for the non-doped clusters. The clusters with the lowest band-gaps, such as $(TiO_2)_4$, $(TiO_2)_6$ and $(TiO_2)_8$, are predicted to be active under irradiation with visible light (600 nm) due to their low values (2 eV). The HOMO-LUMO gap for $(TiO_2)_1$, $(TiO_2)_4$ and $(TiO_2)_{12}$ clusters could not be computed at the HSE06 level due to electronic convergence problems.

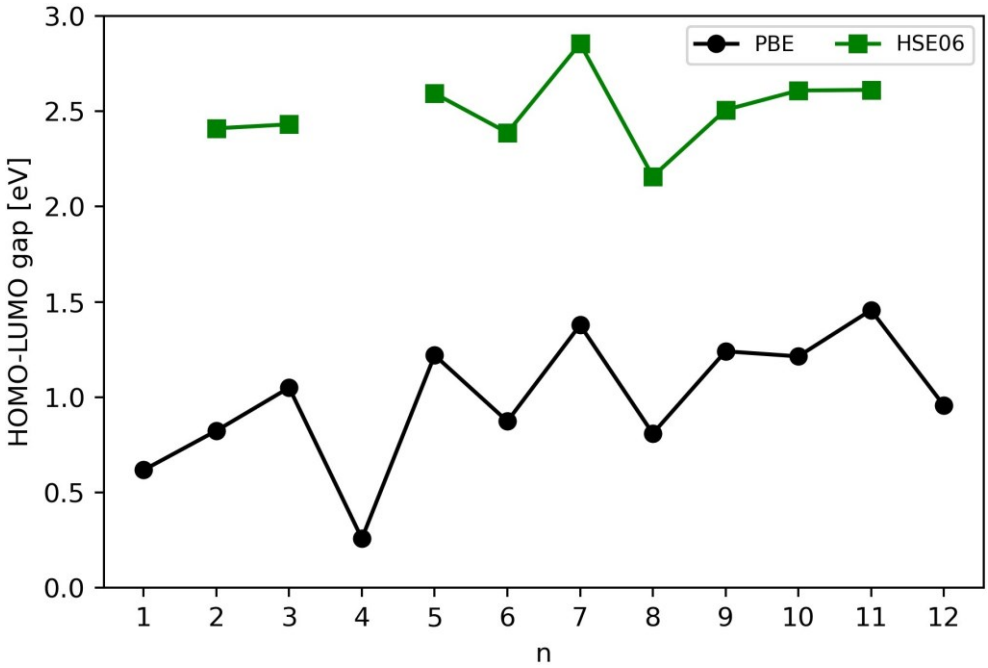

Figure 9: HOMO-LUMO gap of Ru-(TiO_2) clusters relative to the Fermi level (0.0 eV) calculated with the PBE and HSE06 functionals.

In Figure 10 we plot total DOS and PDOS of the Ru-$(TiO_2)_6$ cluster, calculated with the GGA and hybrid level, respectively. We see that Ru *d* states dominate from ~ -2.0 eV up to the Fermi level, which is the reason for the decrease of the band gap. While they are also non-negligible above the Fermi level, this is more evidenced for smaller clusters (such as Ru-$(TiO_2)_3$ as shown in the Supplementary Information). The differences can be explained by the position of the Ru atom. Due to geometric and electronic constraints, in Ru-$(TiO_2)_3$ the single Ru atom is located between the Ti and O atoms, while in Ru-$(TiO_2)_6$ and Ru-$(TiO_2)_{12}$ clusters it preferentially binds to Ti.

Due to different electronegativity of Ti and Ru, there is a net charge transfer. Based on the Bader charge analysis, which is shown in Table 2 for all Ru-$(TiO_2)_n$ clusters ($n = 1 - 12$), Ru atoms donates 0.3–0.6 e_0 electrons to the cluster.

Table 2: Charge transfer from the Ru to the $(TiO_2)_n$ clusters.

n	Δ q [e_0]
1	+ 0.48
2	+ 0.34
3	+ 0.39
4	+ 0.68
5	+ 0.30
6	+ 0.59
7	+ 0.45
8	+ 0.53
9	+ 0.56
10	+0.49
11	+0.48
12	+0.52

It is evident from Table 2 that the charge transfer between Ru atom and TiO_2 clusters occurs from the Ru atom to TiO_2, which is largest for the Ru-$(TiO_2)_4$ cluster and least pronounced for Ru-$(TiO_2)_5$.

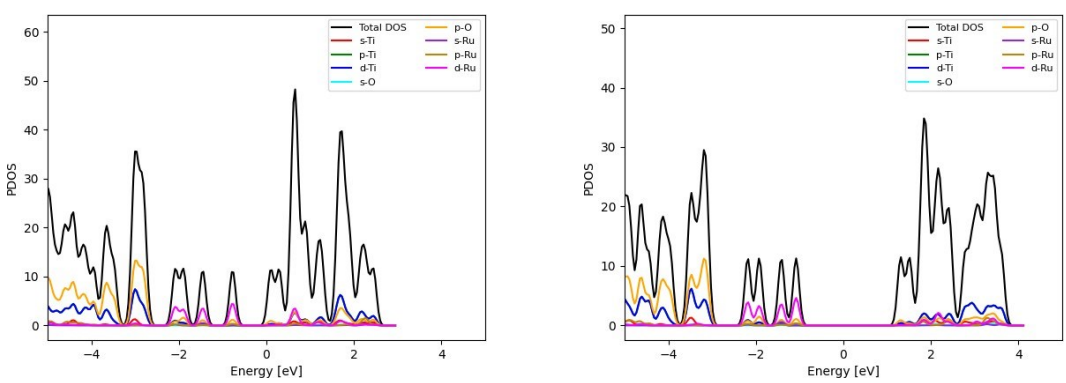

(a) PBE functional

(b) HSE06 functional

Figure 10: Total density of states and projected density of states of the Ru-$(TiO_2)_6$ cluster calculated with a) PBE and b) HSE06 functionals.

3.3. *Adsorption of NRR precursors and products*

For the catalyst to be efficient for NRR, it must bind the reactants sufficiently well. Epitomized by the Sabatier principle, the optimal catalyst should not overbind the substrate [54]. It is known that across analogous reactions the reaction energy generally correlates with the activation energy. In heterogeneous catalysis, this is can be extended to include adsorption energies. This observation is known as the Bronsted-Evans-Polanyi (BEP) correlation and is valid for different types of reactions with varying transferability. While it can be easily ported across different metallic surfaces, it can break for semiconducting oxides, doped materials etc. [55, 56] Conversely, the interaction of the products with the catalyst should be moderate as to avoid catalyst poisoning. Hence, we study the adsorption of N_2, H_2 and NH_3 on the $(TiO_2)_n$ and Ru-$(TiO_2)_n$ clusters ($n = 3, 6, 12$). These were chosen as representative examples of small, medium and large nanoclusters.

The nitrogen molecule (N_2) can adsorb in an end-on or a side-on configuration. In former, only one nitrogen atom is adsorbed at the corresponding active site and the molecule is positioned vertically. The non-adsorbed nitrogen atom is referred to as the distal nitrogen atom. When adsorbed in the side-on configuration, both nitrogen atoms are adsorbed on the active sites of the cluster[16]. The optimized structures for adsorption on the $(TiO_2)_6$ and Ru-$(TiO_2)_6$ clusters are shown in Figures 11 and 13, respectively. For the clusters of other sizes, the reader is referred to the Supplementary Information.

Adsorption energies were calculated at the GGA level (PBE) with and without the Grimme D3 correction because DFT is known to poorly describe the van der Waals dispersion interaction. The calculated adsorption energies are summarized in Figures 12 and 13.

3.3.1. *$(TiO_2)_n$ clusters*

On $(TiO_2)_6$, N_2 preferentially adsorbs in the end-on configuration on the Ti atom with an adsorption energy of -0.41 eV. This has been found to be the lowest adsorption energy among all possible adsorption active sites. Upon adsorption, the molecule geometry remains unperturbed (N-N distance of 1.11 Å). The distance between the Ti atom and the adsorbed N_2 molecule is calculated to be 2.373 Å. As it will be shown later on, there is little overlap between the nitrogen

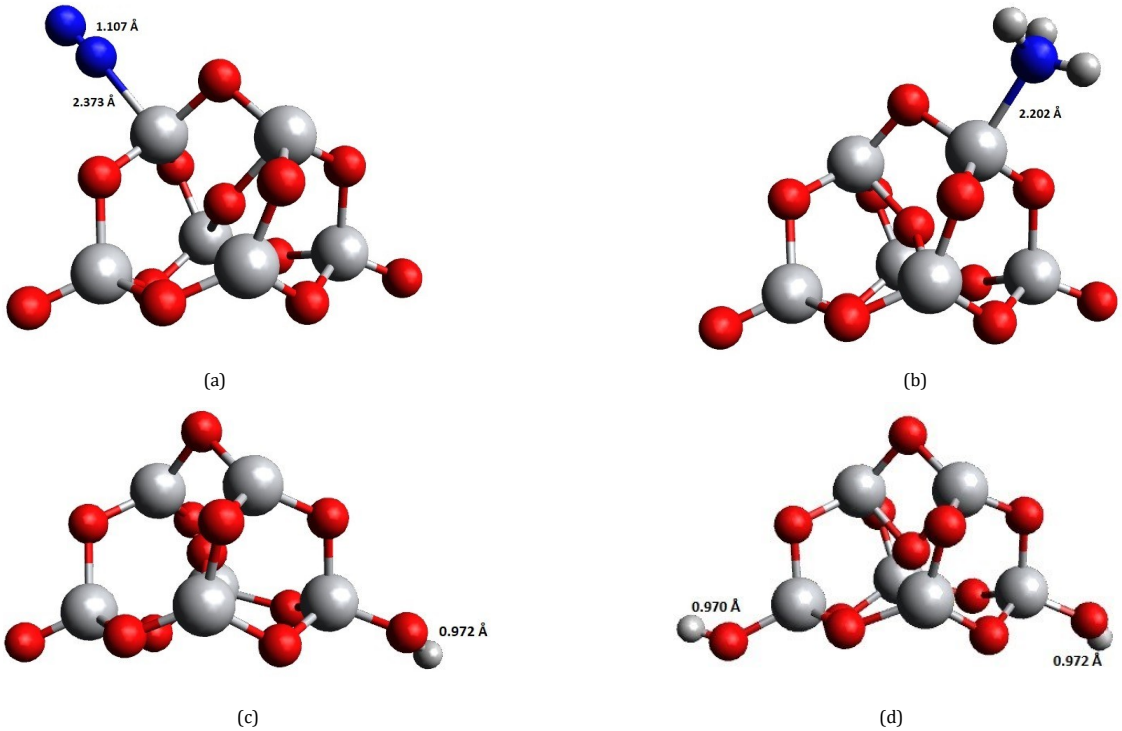

Figure 11: Adsorption modes of a) N_2, b) NH_3, c) H and d) 2 H over $(TiO_2)_6$ cluster.

orbitals and $(TiO_2)_6$ and no charge transfer (Table 3). This indicates that there is little activation of N_2 over the investigated clusters. The side-on adsorption of N_2 was also considered but resulted in negligible interaction (~ -0.05 eV), which was true for the clusters of all sizes. Nevertheless, we observed a clear correlation between the adsorption energies of N_2 and the cluster size, showing that smaller clusters bind N_2 more strongly.

To evaluate the magnitude of the pairing effects, we also tried adsorbing two hydrogen atoms on the cluster. For $(TiO_2)_3$, the effect is small but not negligible. The adsorption energy at the PBE-D3 level decreases from -0.51 eV/atom for 1 H to -0.40 eV/atom for 2 H. However, the observed difference cannot be exclusively ascribed to the pairing effect because the second hydrogen atom is forced in the second most optimal adsorption site. For larger clusters, the difference is negligible (-0.65 eV vs. -0.58 eV and -0.40 eV vs. -0.36 eV for $(TiO_2)_6$ and $(TiO_2)_{12}$, respectively.).

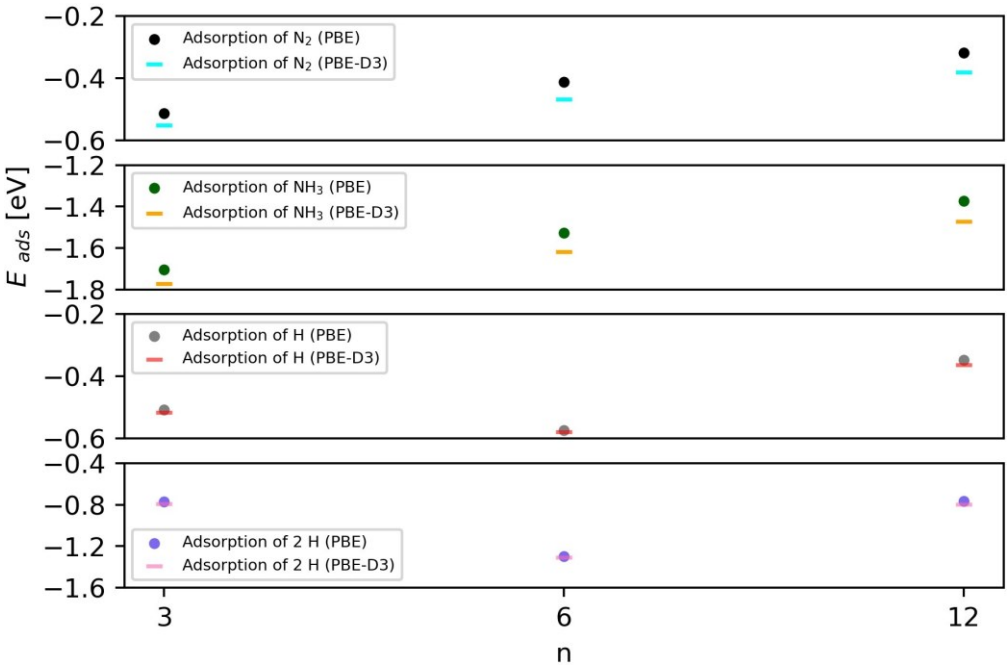

Figure 12: Adsorption energies for adsorption of N_2, NH_3, H and 2 H over $(TiO_2)_n$ clusters (n = 3, 6, 12) calculated with PBE and PBE-D3.

While nitrogen first binds in a molecular form and its dissociation represents the principal bottleneck of the reaction, hydrogen dissociates more readily. Hence, we measure the adsorption energies with respect to gaseous $\frac{1}{2}H_2$. As expected, H atoms preferentially bind to the oxygen atoms in the $(TiO_2)_n$ clusters. The ensuing hydroxyl group is acidic and can give off hydrogen to reduce nitrogen. It was found that the hydrogen atom binds most strongly to terminal oxygen atoms (~ -0.6 eV). Since this interaction is strongly covalent, there is virtually no difference between the PBE and PBE-D3 results. Interestingly, there seems to be a peculiar size effect. Very large ($n = 12$) and very small ($n = 3$) clusters bind hydrogen less strongly than intermediately sized clusters. This is a purely geometric effect, since for $n = 3$ and $n = 12$ there are fewer terminal oxygen atoms and they are less electronegative. In all instances, there is moderate charge transfer from the cluster to the hydrogen atom (0.37 e_0).

Lastly, the adsorption of ammonia as the desired product of NRR was studied. Ammonia adsorbs on a Ti atom quite strongly, reaching −1.7 eV, −1.6 eV and −1.4 eV for $(TiO_2)_3$, $(TiO_2)_6$ and $(TiO_2)_{12}$, respectively. This hints at a strong size effect, where the smaller nanoclusters more strongly adsorb ammonia This interaction is visualized by plotting DOS/PDOS graphs, which can be found in the SI for the adsorption of NH_3 on $(TiO_2)_n$ and also Ru-$(TiO_2)_n$, n=3,6, and 12, clusters. It is clear that overlapping of N atomic orbital of NH3 with Ti d orbitals (LUMO) is more evident in smaller clusters. Due to a strong interaction of Ti *d* orbitals with molecular orbitals from NH_3, the Ti-N distance is reduced to 2.20 Å (which is 0.171 Å shorter than in the N_2 adsorption). In smaller clusters, Ti atoms are undercoordinated and more readily accommodate the valence electron pair from ammonia, which is donated to form the attractive interaction. NH_3 donates 0.12–0.14 e_0 to the cluster upon adsorption.

3.4. Ru-$(TiO_2)_n$ clusters

Doping $(TiO_2)_n$ clusters with Ru imparts electronic changes, which not only move the band-gap from the far UV to the visible part of the spectrum but affect the adsorption of the NRR precursors. Especially transition metals are often introduced into photocatalysts through doping or loading to improve their NRR fixation abilities [13]. For easier comparison, we also studied the adsorption of nitrogen, hydrogen and ammonia over differently sized nanoclusters: Ru-$(TiO_2)_6$ (Figure 13), Ru-$(TiO_2)_3$, and Ru-$(TiO_2)_{12}$.

Accounting for the dispersion interaction through the D3 correction, the adsorption energy of the N_2 adsorbed in the end-on configuration on Ru-$(TiO_2)_6$ is ∼ -1.21 eV, which is 0.75 eV more favorable than adsorption on a pristine TiO_2 cluster. The strong interaction is accompanied with the elongation of the N-N bond (from 1.11 to 1.13 Å), showing activation. The N-Ru distance is calculated to be 1.925 Å (2.373 Å on pristine $(TiO_2)_6$). The side-on mode of adsorption is not stable. Ammonia on the other hand binds with a similar interaction strength than on the pristine cluster (-1.56 eV vs. -1.53 eV). For hydrogen, however, a new adsorption mode is available. While on $(TiO_2)_6$ hydrogen attaches to terminal oxygen atoms, yielding acidic hydroxyl groups, Ru also activates hydrogen. When H adsorbs on Ru (Ru-H distance of 1.589 Å), it is readily available for the

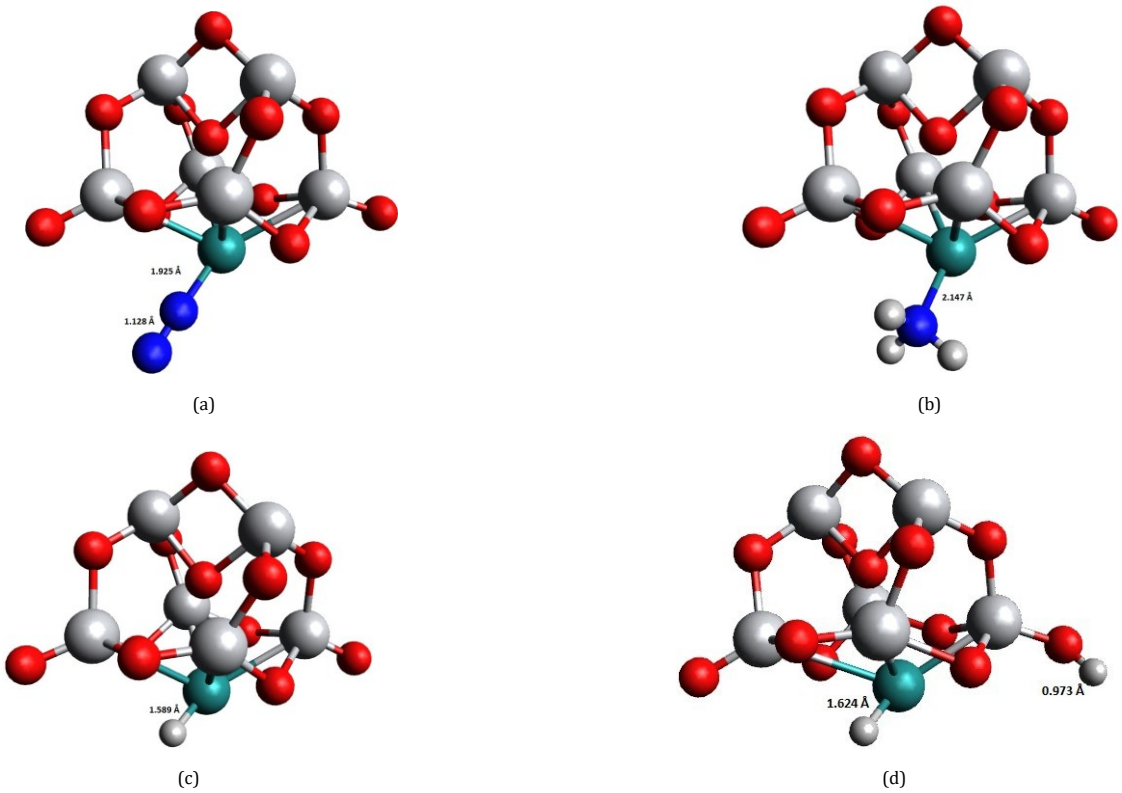

Figure 13: Adsorption modes of a) N_2, b)NH_3, c) H and d) 2 H over Ru-$(TiO_2)_6$ cluster.

reaction (interaction of -0.40 eV). Again, we evaluated the pairing effects, which were notable for Ru-$(TiO_2)_3$ (-0.95 eV vs. -0.68 eV) and Ru-$(TiO_2)_6$ (-0.85 eV vs. -0.49 eV). For larger clusters, the effect is negligible. Accounting for these, the hydrogen adsorption energy monotonically decreases as the cluster size increases.

Compared to Ru-$(TiO_2)_6$, nitrogen and ammonia adsorption on Ru-$(TiO_2)_3$ and Ru-$(TiO_2)_{12}$ occur on the Ru and Ti atoms, respectively. This indicates that Ru is more active in smaller Ru-TiO_2 clusters (n = 3 and 6), while clusters with higher sizes (n = 12) prefer adsorption on Ti. Hydrogen binds to terminal oxygen atom in Ru-$(TiO_2)_3$ but to the adjacent (and not terminal) oxygen atom in Ru-$(TiO_2)_{12}$. For graphical depiction, the reader is referred to the Supplementary Information.

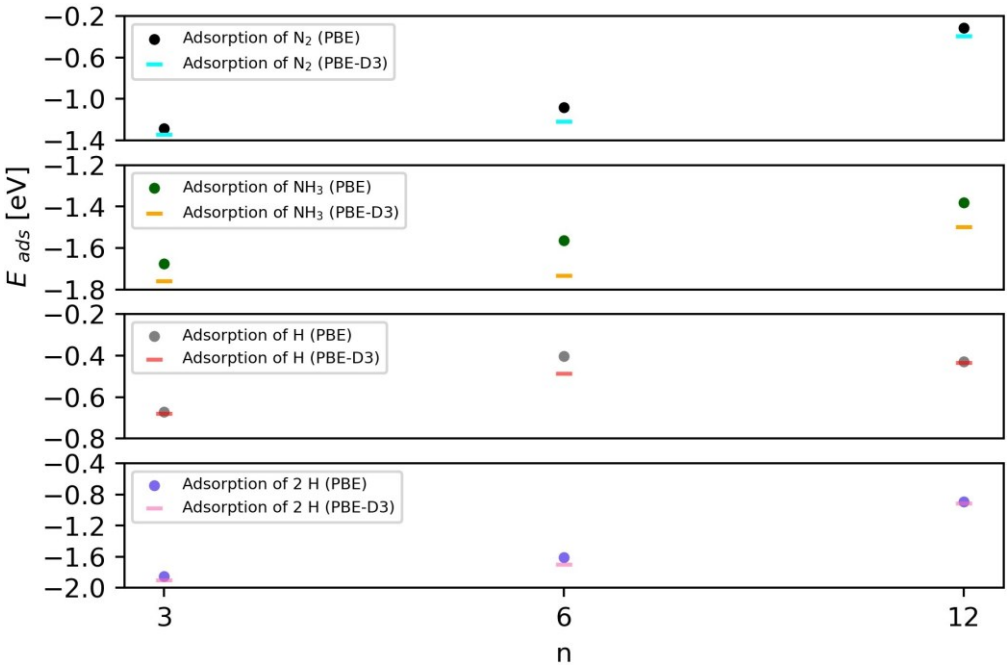

Figure 14: Adsorption energies for adsorption of N_2, NH_3, H and 2 H over Ru-$(TiO_2)_n$ clusters (n = 3, 6, 12) calculated with PBE and PBE-D3.

To further explain the observed difference in adsorption, the Bader charge analysis was perform and charge transfer was calculated (see Table 3). The negligible activation of N_2 on pristine TiO_2 clusters is confirmed by negligible charge transfer between the TiO_2 clusters and adsorbed N_2. On the other hand, N_2 adsorbed on the Ru-TiO_2 clusters abstracts electrons from the catalyst. The effect decreases as the cluster increases, indicating a decreased activation of N_2. The charge transfer from adsorbed NH_3 to the catalyst, i.e., the TiO_2 or Ru-TiO_2 clusters, is constant and similar for adsorption on both types of clusters. When hydrogen binds to Ru, hydrogen abstracts electrons (-0.15 e_0), meaning that a hydride species is available for further reaction.

It should be noted again that Ru-$(TiO_2)_n$ are model systems for photoactive Ru-doped nanocatalysts. In experimental synthesis and under operating conditions, such a fine control is difficult. Clusters can exhibit more dopant atoms, they can agglomerate etc.

Table 3: Charge transfer calculated using Bader charge analysis for the adsorption of N_2, NH_3 and H on TiO_2 and Ru-TiO_2 (n= 3, 6, 12).

	N_2 [e_0]	NH_3 [e_0]	H [e_0]
$(TiO_2)_3$	0.00	+0.12	+0.63
$(TiO_2)_6$	0.00	+0.14	+0.63
$(TiO_2)_{12}$	0.00	+0.13	+0.62
Ru-$(TiO_2)_3$	−0.25	+0.16	+0.64
Ru-$(TiO_2)_6$	−0.20	+0.17	−0.15
Ru-$(TiO_2)_{12}$	0.00	+0.13	+0.60

4. Conclusion

In this study, we studied the electronic properties of TiO_2 and Ru-TiO_2 clusters and determined the adsorption modes of hydrogen, nitrogen and NH_3 using first-principles methods. We investigated the effect of Ru doping and the cluster size effect on the electronic and adsorption properties of the clusters.

First, the most stable $(TiO_2)n$ structures for $n = 1 - 12$ were identified and confirmed using AIMD simulations. Their formation energies and hence their stability increased with the cluster size in a monotonic fashion, approaching the bulk structure in the limit. Furthemore, the clusters were doped with a single Ru atom because of its suitability for the nitrogen reduction reaction. Interestingly, the relative stability of Ru-$(TiO_2)_n$ showed no consistent trend. Ru-$(TiO_2)_5$ was found to exhibit the lowest formation energy and thus greatest stability.

For all the studied clusters, we calculated the following electronic properties: the HOMO-LUMO gap, DOS and PDOS, Bader charge analysis. We show that doping with Ru decreases the HOMO-LUMO gap, allowing the utilization of visible light instead of UV. The DOS and PDOS analyses show that in pristine TiO_2 the bands below the Fermi level consist mainly of oxygen p bands, while the valence levels are contributed by Ti d bands. Ru-loading decreases the HOMO-LUMO gap by changing the electronic structure around the Fermi level due to Ru d electrons.

Lastly, we turn our attention to adsorption. We show that the size of $(TiO_2)_n$ or Ru-$(TiO_2)_n$ clusters as well as Ru loading affect the adsorption of N_2, NH_3 and H. Adsorption properties of small ($n = 3$), medium-sized ($n = 6$) and large ($n = 12$) clusters were studied. On TiO_2

clusters, N_2 and NH_3 bind on Ti atoms, while hydrogen preferentially attaches to terminal oxygen atoms, forming acidic hydroxyl groups. On smaller Ru-$(TiO_2)_n$ clusters, NH_3, N_2 and hydrogen bind through Ru. While TiO_2 only physisorbs nitrogen, Ru-TiO_2 forms a stronger chemisorption interaction, which is evidenced by an orbital overlap, large charge transfer and bond elongation. On larger clusters (n = 12), Ti atoms adsorb NH_3 and N_2.

Charge transfer during the adsorption was also confirmed by calculating the Bader charges, which revealed that N_2 adsorbed on the Ru active site of the Ru-$(TiO_2)_3$ and Ru-$(TiO_2)_6$ clusters abstracts electrons from the catalyst. Injection of the electrons in the antiboding orbital of nitrogen is consistent with the elongation of the triple bond, indicating nitrogen activation. In general, both the electronic and adsorption properties of Ru-TiO_2 clusters (compared to pristine clusters) show a favorable effect of Ru loading on the N_2 fixation ability and its consequent activation. While Ru doping improves nitrogen adsorption and activation on TiO_2 clusters, the adsorption interaction of hydrogen and ammonia remains relatively unchanged. This is particularly beneficial for NRR, since high coverages of hydrogen or products (ammonia) decrease the performance of catalysts.

This study of nitrogen activation on TiO_2 clusters shows that benefits of Ru doping. Moreover, it shows that the stability of differently sized clusters is not a monotonous function of size, as naively expected, and pinpoints which clusters are promising candidates for photocatalytic nitrogen activation on nanoclusters.

5. Acknowledgements

This work was supported by the Slovenian Research Agency (Grant P2-0152). B.L. was funded by a research project (Grant N2-0135), T.Ž. was funded by core funding (Grant P1-0418) and M.H. was funded by core funding (Grant P2-0421). Infrastructure funding (Grant I0-0039) from the Slovenian Research Agency is also acknowledged.

References

[1] J. W. Erisman, M. A. Sutton, J. Galloway, Z. Klimont, W. Winiwarter, How a century of ammonia synthesis changed the world, Nature Geoscience 1 (10) (2008) 636–639. doi:

10.1038/ngeo325.

[2] C. Smith, A. K. Hill, L. Torrente-Murciano, Current and future role of Haber–Bosch ammonia in a carbon-free energy landscape, Energy & Environmental Science 13 (2) (2020) 331–344. doi:10.1039/c9ee02873k.

[3] V. Kyriakou, I. Garagounis, A. Vourros, E. Vasileiou, M. Stoukides, An Electrochemical Haber–Bosch Process, Joule 4 (1) (2020) 142–158. doi:10.1016/j.joule.2019.10.006.

[4] M. Li, H. Huang, J. Low, C. Gao, R. Long, Y. Xiong, Recent Progress on Electrocatalyst and Photocatalyst Design for Nitrogen Reduction, Small Methods 3 (6) (2018) 1800388. doi:10.1002/smtd.201800388.

[5] R. Shi, X. Zhang, G. I. N. Waterhouse, Y. Zhao, T. Zhang, The Journey toward Low Temperature, Low Pressure Catalytic Nitrogen Fixation, Advanced Energy Materials 10 (19) (2020) 2000659. doi:10.1002/aenm.202000659.

[6] R. Shi, Y. Zhao, G. I. N. Waterhouse, S. Zhang, T. Zhang, Defect Engineering in Photocatalytic Nitrogen Fixation, ACS Catalysis 9 (11) (2019) 9739–9750. doi:10.1021/acscatal.9b03246.

[7] H. Li, C. Mao, H. Shang, Z. Yang, Z. Ai, L. Zhang, New opportunities for efficient N_2 fixation by nanosheet photocatalysts, Nanoscale 10 (33) (2018) 15429–15435. doi:10.1039/c8nr04277b.

[8] I. Ali, M. Suhail, Z. A. Alothman, A. Alwarthan, Recent advances in syntheses, properties and applications of TiO_2 nanostructures, RSC Advances 8 (53) (2018) 30125–30147. doi:10.1039/c8ra06517a.

[9] Ž. Kovačič, B. Likozar, M. Huš, Photocatalytic CO_2 Reduction: A Review of Ab Initio Mechanism, Kinetics, and Multiscale Modeling Simulations, ACS Catalysis 10 (24) (2020) 14984–15007. doi:10.1021/acscatal.0c02557.

[10] D. Çakır, O. Gülseren, Ab initiostudy of neutral $(TiO_2)_n$ clusters and their interactions with

water and transition metal atoms, Journal of Physics: Condensed Matter 24 (30) (2012) 305301. doi:10.1088/0953-8984/24/30/305301.

[11] A. Fujishima, K. Honda, Electrochemical Photolysis of Water at a Semiconductor Electrode, Nature 238 (5358) (1972) 37–38. doi:10.1038/238037a0.

[12] M. Ni, M. K. Leung, D. Y. Leung, K. Sumathy, An review and recent developments in photocatalytic water-splitting using TiO_2 for hydrogen production, Renewable and Sustainable Energy Reviews 11 (3) (2007) 401–425. doi:10.1016/j.rser.2005.01.009.

[13] R. Huang, X. Li, W. Gao, X. Zhang, S. Liang, M. Luo, Recent advances in photocatalytic nitrogen fixation: from active sites to ammonia quantification methods, RSC Advances 11 (24) (2021) 14844–14861. doi:10.1039/d0ra10439f.

[14] D. O. Scanlon, C. W. Dunnill, J. Buckeridge, S. A. Shevlin, A. J. Logsdail, S. M. Woodley, C. R. A. Catlow, M. J. Powell, R. G. Palgrave, I. P. Parkin, G. W. Watson, T. W. Keal, P. Sherwood, A. Walsh, A. A. Sokol, Band alignment of rutile and anatase TiO_2, Nature Materials 12 (9) (2013) 798–801. doi:10.1038/nmat3697.

[15] G. N. Schrauzer, T. D. Guth, Photolysis of Water and Photoreduction of Nitrogen on Titanium Dioxide, Journal of the American Chemical Society 99 (22) (1977) 7189–7193. doi:10.1021/ja00464a015.

[16] K. Ithisuphalap, H. Zhang, L. Guo, Q. Yang, H. Yang, G. Wu, Photocatalysis and Photoelectrocatalysis Methods of Nitrogen Reduction for Sustainable Ammonia Synthesis, Small Methods 3 (6) (2018) 1800352. doi:10.1002/smtd.201800352.

[17] X.-Y. Xie, P. Xiao, W.-H. Fang, G. Cui, W. Thiel, Probing Photocatalytic Nitrogen Reduction to Ammonia with Water on the Rutile TiO_2 (110) Surface by First-Principles Calculations, ACS Catalysis 9 (10) (2019) 9178–9187. doi:10.1021/acscatal.9b01551.

[18] W. Zhao, J. Zhang, X. Zhu, M. Zhang, J. Tang, M. Tan, Y. Wang, Enhanced nitrogen photofixation on Fe-doped TiO_2 with highly exposed (101) facets in the presence of ethanol as scav-

enger, Applied Catalysis B: Environmental 144 (2014) 468–477. doi:10.1016/j.apcatb.2013.07.047.

[19] R. Guan, D. Wang, Y. Zhang, C. Liu, W. Xu, J. Wang, Z. Zhao, M. Feng, Q. Shang, Z. Sun, Enhanced photocatalytic N_2 fixation via defective and fluoride modified TiO_2 surface, Applied Catalysis B: Environmental 282 (2021) 119580. doi:10.1016/j.apcatb.2020.119580.

[20] Y. Zhang, X. Chen, S. Zhang, L. Yin, Y. Yang, Defective titanium dioxide nanobamboo arrays architecture for photocatalytic nitrogen fixation up to 780 nm, Chemical Engineering Journal 401 (2020) 126033. doi:10.1016/j.cej.2020.126033.

[21] W. Gao, X. Li, S. Luo, Z. Luo, X. Zhang, R. Huang, M. Luo, In situ modification of cobalt on MXene/TiO_2 as composite photocatalyst for efficient nitrogen fixation, Journal of Colloid and Interface Science 585 (2021) 20–29. doi:10.1016/j.jcis.2020.11.064.

[22] J. Li, D. Wang, R. Guan, Y. Zhang, Z. Zhao, H. Zhai, Z. Sun, Vacancy-Enabled Mesoporous TiO_2 Modulated by Nickel Doping with Enhanced Photocatalytic Nitrogen Fixation Performance, ACS Sustainable Chemistry & Engineering 8 (49) (2020) 18258–18265. doi:10.1021/acssuschemeng.0c06775.

[23] Y. Sun, W. Pei, M. Xie, S. Xu, S. Zhou, J. Zhao, K. Xiao, Y. Zhu, Excitonic $Au_4Ru_2(PPh_3)_2(SC_2H_4Ph)_8$ cluster for light-driven dinitrogen fixation, Chemical Science 11 (9) (2020) 2440–2447. doi:10.1039/c9sc06424a.

[24] J. Qian, S. Zhao, W. Dang, Y. Liao, W. Zhang, H. Wang, L. Lv, L. Luo, H.-Y. Jiang, J. Tang, Photocatalytic Nitrogen Reduction by Ti_3C_2 MXene Derived Oxygen Vacancy-Rich C/TiO_2, Advanced Sustainable Systems 5 (4) (2021) 2000282. doi:10.1002/adsu.202000282.

[25] W. Ye, M. Arif, X. Fang, M. A. Mushtaq, X. Chen, D. Yan, Efficient Photoelectrochemical Route for the Ambient Reduction of N_2 to NH_3 Based on Nanojunctions Assembled from MoS_2 Nanosheets and TiO_2, ACS Applied Materials & Interfaces 11 (32) (2019) 28809–28817. doi:10.1021/acsami.9b06596.

[26] B. Huang, Y. Liu, Q. Pang, X. Zhang, H. Wang, P. K. Shen, Boosting the photocatalytic activity of mesoporous $SrTiO_3$ for nitrogen fixation through multiple defects and strain engineering, Journal of Materials Chemistry A 8 (42) (2020) 22251–22256. doi:10.1039/d0ta08678a.

[27] Z. Zhao, D. Wang, R. Gao, G. Wen, M. Feng, G. Song, J. Zhu, D. Luo, H. Tan, X. Ge, W. Zhang, Y. Zhang, L. Zheng, H. Li, Z. Chen, Magnetic-Field-Stimulated Efficient Photocatalytic N_2 Fixation over Defective $BaTiO_3$ Perovskites, Angewandte Chemie International Edition 60 (21) (2021) 11910–11918. doi:10.1002/anie.202100726.

[28] C. Li, T. Wang, Z.-J. Zhao, W. Yang, J.-F. Li, A. Li, Z. Yang, G. A. Ozin, J. Gong, Promoted Fixation of Molecular Nitrogen with Surface Oxygen Vacancies on Plasmon-Enhanced TiO_2 Photoelectrodes, Angewandte Chemie International Edition 57 (19) (2018) 5278–5282. doi:10.1002/anie.201713229.

[29] Y. Zhao, Y. Zhao, R. Shi, B. Wang, G. I. N. Waterhouse, L.-Z. Wu, C.-H. Tung, T. Zhang, Tuning Oxygen Vacancies in Ultrathin TiO_2 Nanosheets to Boost Photocatalytic Nitrogen Fixation up to 700 nm, Advanced Materials 31 (16) (2019) 1806482. doi:10.1002/adma.201806482.

[30] J. Yang, Y. Guo, R. Jiang, F. Qin, H. Zhang, W. Lu, J. Wang, J. C. Yu, High-Efficiency "Working-in-Tandem" Nitrogen Photofixation Achieved by Assembling Plasmonic Gold Nanocrystals on Ultrathin Titania Nanosheets, Journal of the American Chemical Society 140 (27) (2018) 8497–8508. doi:10.1021/jacs.8b03537.

[31] G. Zhang, X. Yang, C. He, P. Zhang, H. Mi, Constructing a tunable defect structure in TiO_2 for photocatalytic nitrogen fixation, Journal of Materials Chemistry A 8 (1) (2020) 334–341. doi:10.1039/c9ta10471b.

[32] T. Hou, Q. Li, Y. Zhang, W. Zhu, K. Yu, S. Wang, Q. Xu, S. Liang, L. Wang, Near-infrared light-driven photofixation of nitrogen over $Ti_3C_2T_x/TiO_2$ hybrid structures with superior activity and stability, Applied Catalysis B: Environmental 273 (2020) 119072. doi:10.1016/j.apcatb.2020.119072.

[33] S. Liu, Y. Wang, S. Wang, M. You, S. Hong, T.-S. Wu, Y.-L. Soo, Z. Zhao, G. Jiang, J. Qiu, B. Wang, Z. Sun, Photocatalytic Fixation of Nitrogen to Ammonia by Single Ru Atom Decorated TiO_2 Nanosheets, ACS Sustainable Chemistry & Engineering 7 (7) (2019) 6813–6820. doi:10.1021/acssuschemeng.8b06134.

[34] B. M. Comer, Y.-H. Liu, M. B. Dixit, K. B. Hatzell, Y. Ye, E. J. Crumlin, M. C. Hatzell, A. J. Medford, The Role of Adventitious Carbon in Photo-catalytic Nitrogen Fixation by Titania, Journal of the American Chemical Society 140 (45) (2018) 15157–15160. doi:10.1021/jacs.8b08464.

[35] Y. Liao, J. Qian, G. Xie, Q. Han, W. Dang, Y. Wang, L. Lv, S. Zhao, L. Luo, W. Zhang, H.-Y. Jiang, J. Tang, 2D-layered Ti_3C_2 MXenes for promoted synthesis of NH_3 on P25 photocatalysts, Applied Catalysis B: Environmental 273 (2020) 119054. doi:10.1016/j.apcatb.2020.119054.

[36] B. M. Comer, A. J. Medford, Analysis of Photocatalytic Nitrogen Fixation on Rutile TiO_2 (110), ACS Sustainable Chemistry & Engineering 6 (4) (2018) 4648–4660. doi:10.1021/acssuschemeng.7b03652.

[37] S. Ghoshal, A. Pramanik, P. Sarkar, Towards H_2O catalyzed N_2-fixation over TiO_2 doped Ru_n clusters (n = 5, 6): a mechanistic and kinetic approach, Physical Chemistry Chemical Physics 23 (2) (2021) 1527–1538. doi:10.1039/d0cp03507f.

[38] J. J. Mortensen, L. B. Hansen, K. W. Jacobsen, Real-space grid implementation of the projector augmented wave method, Physical Review B 71 (3) (2005) 035109. doi:10.1103/physrevb.71.035109.

[39] J. Enkovaara, C. Rostgaard, J. J. Mortensen, J. Chen, M. Dułak, L. Ferrighi, J. Gavnholt, C. Glinsvad, V. Haikola, H. A. Hansen, H. H. Kristoffersen, M. Kuisma, A. H. Larsen, L. Lehtovaara, M. Ljungberg, O. Lopez-Acevedo, P. G. Moses, J. Ojanen, T. Olsen, V. Petzold, N. A. Romero, J. Stausholm-Møller, M. Strange, G. A. Tritsaris, M. Vanin, M. Walter, B. Hammer, H. Häkkinen, G. K. H. Madsen, R. M. Nieminen, J. K. Nørskov, M. Puska, T. T. Rantala, J. Schiøtz, K. S. Thygesen, K. W. Jacobsen, Electronic structure calculations with GPAW:

a real-space implementation of the projector augmented-wave method, Journal of Physics: Condensed Matter 22 (25) (2010) 253202. doi:10.1088/0953-8984/22/25/253202.

[40] M. Ernzerhof, G. E. Scuseria, Assessment of the Perdew–Burke–Ernzerhof exchange-correlation functional, The Journal of Chemical Physics 110 (11) (1999) 5029–5036. doi:10.1063/1.478401.

[41] J. Heyd, G. E. Scuseria, Efficient hybrid density functional calculations in solids: Assessment of the Heyd–Scuseria–Ernzerhof screened Coulomb hybrid functional, The Journal of Chemical Physics 121 (3) (2004) 1187–1192. doi:10.1063/1.1760074.

[42] P. J. Hasnip, K. Refson, M. I. J. Probert, J. R. Yates, S. J. Clark, C. J. Pickard, Density functional theory in the solid state, Philosophical Transactions of the Royal Society A: Mathematical, Physical and Engineering Sciences 372 (2011) (2014) 20130270. doi:10.1098/rsta.2013.0270.

[43] J. L. Bao, L. Gagliardi, D. G. Truhlar, Self-Interaction Error in Density Functional Theory: An Appraisal, The Journal of Physical Chemistry Letters 9 (9) (2018) 2353–2358. doi:10.1021/acs.jpclett.8b00242.

[44] E. Berardo, H.-S. Hu, S. A. Shevlin, S. M. Woodley, K. Kowalski, M. A. Zwijnenburg, Modeling Excited States in TiO_2 Nanoparticles: On the Accuracy of a TD-DFT Based Description, Journal of Chemical Theory and Computation 10 (3) (2014) 1189–1199. doi:10.1021/ct4010273.

[45] J. Zhang, M. Dolg, ABCluster: the artificial bee colony algorithm for cluster global optimization, Physical Chemistry Chemical Physics 17 (37) (2015) 24173–24181. doi:10.1039/c5cp04060d.

[46] J. Zhang, M. Dolg, Global optimization of clusters of rigid molecules using the artificial bee colony algorithm, Physical Chemistry Chemical Physics 18 (4) (2016) 3003–3010. doi:10.1039/c5cp06313b.

[47] J. Zhang, V.-A. Glezakou, R. Rousseau, M.-T. Nguyen, NWPEsSe: An Adaptive-Learning Global Optimization Algorithm for Nanosized Cluster Systems, Journal of Chemical Theory and Computation 16 (6) (2020) 3947–3958. doi:10.1021/acs.jctc.9b01107.

[48] A. M. Doyle, S. K. Shaikhutdinov, S. D. Jackson, H.-J. Freund, Hydrogenation on Metal Surfaces: Why are Nanoparticles More Active than Single Crystals?, Angewandte Chemie International Edition 42 (42) (2003) 5240–5243. doi:10.1002/anie.200352124.

[49] D. Kopač, B. Likozar, M. Huš, How Size Matters: Electronic, Cooperative, and Geometric Effect in Perovskite-Supported Copper Catalysts for CO_2 Reduction, ACS Catalysis 10 (7) (2020) 4092–4102. doi:10.1021/acscatal.9b05303.

[50] J.-L. Bredas, Mind the gap!, Mater. Horiz. 1 (1) (2014) 17–19. doi:10.1039/c3mh00098b.

[51] J. Gomes, A. Lopes, K. Bednarczyk, M. Gmurek, M. Stelmachowski, A. Zaleska-Medynska, M. Quinta-Ferreira, R. Costa, R. Quinta-Ferreira, R. Martins, Effect of Noble Metals (Ag, Pd, Pt) Loading over the Efficiency of TiO_2 during Photocatalytic Ozonation on the Toxicity of Parabens, ChemEngineering 2 (1) (2018) 4. doi:10.3390/chemengineering2010004.

[52] T. Luttrell, S. Halpegamage, J. Tao, A. Kramer, E. Sutter, M. Batzill, Why is anatase a better photocatalyst than rutile? - Model studies on epitaxial TiO_2 films, Scientific Reports 4 (1) (feb 2014). doi:10.1038/srep04043.

[53] M. Landmann, E. Rauls, W. G. Schmidt, The electronic structure and optical response of rutile, anatase and brookite TiO_2, Journal of Physics: Condensed Matter 24 (19) (2012) 195503. doi:10.1088/0953-8984/24/19/195503.

[54] A. J. Medford, A. Vojvodic, J. S. Hummelshøj, J. Voss, F. Abild-Pedersen, F. Studt, T. Bligaard, A. Nilsson, J. K. Nørskov, From the Sabatier principle to a predictive theory of transition-metal heterogeneous catalysis, Journal of Catalysis 328 (2015) 36–42. doi:10.1016/j.jcat.2014.12.033.

[55] T. Bligaard, J. Nørskov, S. Dahl, J. Matthiesen, C. Christensen, J. Sehested, The Brønsted–Evans–Polanyi relation and the volcano curve in heterogeneous catalysis, Journal of Catalysis 224 (1) (2004) 206–217. doi:10.1016/j.jcat.2004.02.034.

[56] C. J. H. Jacobsen, S. Dahl, B. S. Clausen, S. Bahn, A. Logadottir, J. K. Nørskov, Catalyst Design by Interpolation in the Periodic Table: Bimetallic Ammonia Synthesis Catalysts, Journal of the American Chemical Society 123 (34) (2001) 8404–8405. doi:10.1021/ja010963d.